PROCEEDINGS OF SPIE

SPIEDigitalLibrary.org/conference-proceedings-of-spie

Dual-modal photoacoustic and ultrasound microscopy using optically-transparent and high-NA PVDF transducer

Cheng Fang, Jun Zou

Cheng Fang, Jun Zou, "Dual-modal photoacoustic and ultrasound microscopy using optically-transparent and high-NA PVDF transducer," Proc. SPIE 11960, Photons Plus Ultrasound: Imaging and Sensing 2022, 1196019 (3 March 2022); doi: 10.1117/12.2607808

SPIE.

Event: SPIE BiOS, 2022, San Francisco, California, United States

Dual-Modal Photoacoustic and Ultrasound Microscopy Using Optically-Transparent and High-NA PVDF Transducer

Cheng Fang, Jun Zou
Dept. of Electrical and Computer Engineering, Texas A&M University, College Station, TX, USA 77843-3128

ABSTRACT

As two important acoustic imaging modalities, photoacoustic microscopy (PAM) and ultrasound microscopy (UM) provide complementary functional and structural information on biological tissues. At penetration depths beyond the optical diffraction limit, the spatial resolution of both PAM and UM is determined acoustically by the receiving (focused) ultrasound transducer. To obtain good dual-modal imaging resolution, the transducer should have a high center frequency with a wide bandwidth. More importantly, a high acoustic numerical aperture (NA) should be maintained for receiving the PA and ultrasound signals, which is however difficult to achieve as the light blockage by the transducer is more likely to occur at higher NAs. In this paper, we report the dual-modal PAM and UM based on an optically-transparent focused PVDF transducer with a high NA of 0.64. The transducer has an acoustic center frequency and bandwidth of 36 MHz and 44 MHz, respectively. The acoustic focal diameter and zone are 37.8 μm and 210 μm, respectively. With a central transparent window, the excitation laser pulses can directly pass through the transducer to illuminate the target. This allows a high acoustic NA to be obtained without light blockage. For demonstration, co-registered 3D and 2D PAM/UM imaging experiments have been conducted on a twisted wire target in both water and chicken breast tissue, and in-vivo on a mouse tail, respectively. The imaging results show that high acoustic resolution and sensitivity can be achieved to resolve the target at different depths with a simple and compact dual-modal imaging setup.

Keywords: Photoacoustic microscopy, ultrasound microscopy, optically-transparent transducer, high numerical aperture

1. INTRODUCTION

As a hybrid imaging modality, photoacoustic microscopy (PAM) combines optical absorption contrasts with acoustic detection of laser-generated ultrasound signals (i.e., photoacoustic (PA) signals) [1] [2]. Because the light for PA excitation will be highly scattered beyond the optical diffraction limit in tissues, the spatial resolution of PAM will be mainly determined acoustically by the receiving (focused) ultrasound transducer. PAM operating in this regime is termed as acoustic-resolution PAM (AR-PAM). To obtain good AR-PAM resolution, the acoustic focal spot and zone of the receiving transducer need to be minimized. To achieve this, the transducer should operate at high frequencies with a wide bandwidth, and also have a high acoustic numerical aperture (NA). However, this causes a fundamental challenge in the (AR-)PAM system design, as the excitation light can be easily blocked by the transducer. Although a transmission mode (where the optical excitation and acoustic detection are arranged on the opposite sides of the target) can be adopted to circumvent this issue, it is not practical for imaging thicker targets oftentimes encountered under *in-vivo* conditions.

To address this issue, a dark-field setup [3] and opto-acoustic combiner [4] [5] have been developed to separate the optical and acoustic paths, which however make the PA scanning head complex (Figs. 1 (a) and (b)). Alternatively, focused hollow transducers [6] and planar transparent transducers [7] [8] [9] allow the laser to directly pass through. Nevertheless, with the center part removed or without a well-defined acoustic focal point, their acoustic sensitivity and focusing capability are compromised, which make them unsuitable for AR-PAM. Recently, AR-PAM based on an optically-transparent focused transducer has been reported [10] [11](Fig. 1 (c)). Different from the hollow transducers, the transparent transducer still maintains a full acoustic receiving aperture, while allowing the excitation light to transmit through the transparent window. Nevertheless, limited by the narrow bandwidth caused by the hard piezoelectric material and non-ideal backing, optimal imaging resolution has not been achieved. Previously, we reported an optically-transparent focused polyvinylidene fluoride (PVDF) transducer laminated onto a concave glass lens (Fig. 1 (d)) [12]. However, due to the remaining issues in the fabrication process, only a low (acoustic) NA of 0.23 was obtained, which is not sufficient to provide the needed lateral resolution for AR-PAM.

Photons Plus Ultrasound: Imaging and Sensing 2022, edited by Alexander A. Oraevsky, Lihong V. Wang
Proc. of SPIE Vol. 11960, 1196019 · © 2022 SPIE · 1605-7422 · doi: 10.1117/12.2607808

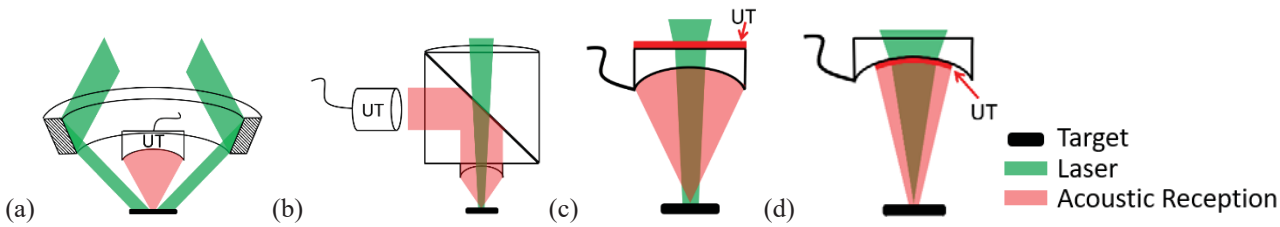

Figure 1. Schematics of current (reflection-mode) AR-PAM setups based on (a) dark-field illumination, (b) opto-acoustic combiners, (c) focused transparent transducer with acoustic lens, (d) previous low-NA focused PVDF transducer. UT: ultrasound transducer.

In this paper, we report the dual-modal (AR-)PAM and UM based on a new optically-transparent focused PVDF transducer. Owing to the improved fabrication process, the new transducer has a much higher (acoustic) NA of 0.64, and also higher center frequency and wider bandwidth than the previous low-NA PVDF transducer (together with other comparable transducers) [13]. For demonstration, a dual-modal PAM and UM setup has been built, and imaging experiments have been conducted on a twisted wire target in water and chicken breast tissue, and *in-vivo* on a mouse tail. The imaging results show that high acoustic resolution and sensitivity can be achieved with a simple and compact setup to resolve the target at different depths beyond the optical diffraction limit.

2. TRANSDUCER DESIGN AND CONSTRUCTION

Fig. 2 shows the schematic design of the high-NA optically-transparent PVDF transducer. The 9-μm-thick PVDF film is molded onto the spherical surface of a plano-concave glass lens with a diameter of 12.0 mm and a spherical radius (acoustic focal length) of 9.4 mm, which corresponds to an acoustic NA of 0.64. The central transparent region (with a diameter of 3.0 mm) of the transducer is covered with ITO (indium-tin oxide) electrodes, while the remaining portion has chromium/copper electrodes to reduce the electrical resistance. The optical transmittance of the central transparent region is around 60% at 532 nm [12]. In order to build the high-NA transducer with a well-defined acoustic focal point, two major improvements have been made in the fabrication process. First, a two-step molding process using one low-NA (~0.49) and then one high-NA (~0.64) lens pairs is employed to address the wrinkling issue on the outer edge of the previous transducer [12], which is the main limiting factor to achieve high NA. Second, after the bonding, a degassing procedure is performed in a vacuum chamber to remove any trapped gas bubbles underneath the PVDF film before the epoxy is fully cured, which is the secondary limiting factor to achieve high NA. With the above two improvements, a larger and better-formed spherical PVDF film is obtained to enable the higher NA and also better acoustic performance not achieved in the previous work.

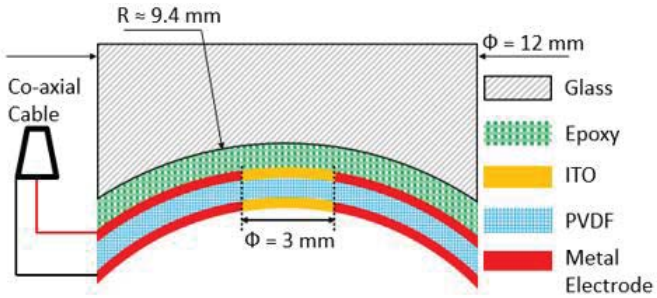

Figure 2. Schematic design of the high-NA transparent PVDF transducer.

3. TRANSDUCER TESTING AND CHARACTERIZATION

A combined PA and pulse-echo ultrasound testing setup was built to characterize the acoustic performance of the high-NA transparent PVDF transducer by using a razor blade in water (whose edge was coated with black ink) as the target (Fig. 3). The front spherical surface of the transducer was immersed in water and the target was placed onto a computer-controlled two-axis motor stage and a manually-adjusted height stage. For PA testing, the light source is a 532-nm pulsed laser (Elforlight, UK) triggered by a function generator with a 1-kHz repetition frequency. The output laser beam was

expanded, passed through a beam splitter, reflected by a stationary mirror, and focused by a lens with 10-cm focal length. The loosely focused laser beam propagated through the transducer with effective optical focal length around -16 mm from air to water and was incident onto the target. A CCD camera was used to monitor the excitation region through the reverse path of the optical illumination. Laser pulse energy after the transparent transducer was measured to be 35 μJ, and the laser beam diameter on the top surface of the target was around 1 mm, which corresponds to a laser intensity of 4.5 mJ/cm^2, far below the ANSI limit of 20 mJ/cm^2. The transducer was connected to a pulser-receiver, which sends electrical voltage pulses to the transducer (for pulse-echo ultrasound testing and imaging), and also amplify the ultrasound and PA signals received by the transducer. The pulse-echo ultrasound axial resolution was quantified by the minimal FWHM (full width at half maximum) of the signal envelope in the depth direction, which was calculated by the absolute Hilbert transformation. The acoustic focal spot was characterized by the minimal FWHM of the amplitude profile in the lateral direction, and the acoustic depth of focus was estimated by the height range where the on-axis peak amplitude dropped to half of its maximal value [14]. To characterize the sensitivity of the high-NA transparent PVDF transducer, a needle hydrophone (Precision Acoustics, UK) with sensitivity (or conversion factor) 60 mV/MPa served as the reference. The characterized main acoustic parameters of the high-NA transparent PVDF transducer are listed in Table 1.

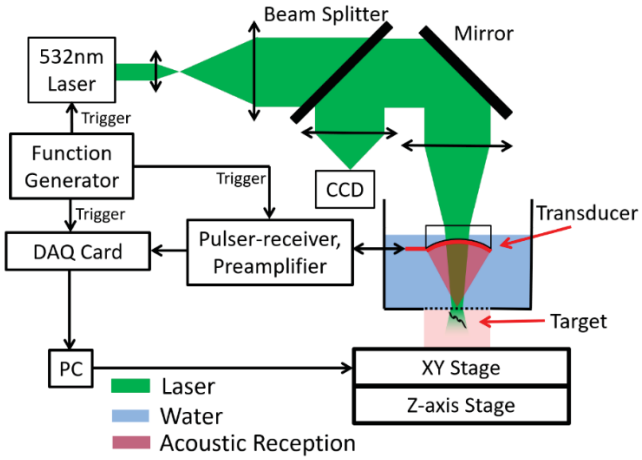

Figure 3. Schematic of the dual-modal PAM and UM setup with the high-NA transparent PVDF transducer.

Table 1. The characterized main acoustic parameters of the high-NA transparent PVDF transducer. US: ultrasound.

Parameter	Value
Acoustic Numerical Aperture (NA)	0.64
PA Axial Resolution	39.1 μm
Center Frequency (f_c)	36 MHz
Bandwidth (BW)	44 MHz
US Pulse-echo Lateral Resolution (Focal Spot Diameter)	37.8 μm
US Pulse-echo Axial Resolution	17.7 μm
US Pulse-echo Depth of Focus	210 μm
Sensitivity or Conversion Factor	3.06 μV/Pa
Noise-equivalent Pressure	48.5 Pa

4. IMAGING EXPERIMENTS AND RESULTS

The experimental setup (Fig. 3) was also used to demonstrate the PA and ultrasound imaging capability of the high-NA transparent PVDF transducer. Because the laser illumination spot is much larger than the acoustic focal spot of the transducer, the imaging resolution is determined acoustically by the focal spot of the transducer. The high-NA transparent PVDF transducer collected both PA and pulse-echo ultrasound signals from the target (Fig. 4). The reconstructed ultrasound image served as a reference for evaluating the PA image. The pulser-receiver was synchronously triggered by the function generator to drive the transducer for sending ultrasound pulses to the target. One trigger from the function generator initiated simultaneous PA and ultrasound data acquisition. It should be noted that the single triggering scheme will not cause the mixing of PA and ultrasound signals. Upon excitation, the ultrasound signal goes through a round trip (from the target to the transducer) and reaches the transducer, while the PA signal arrives after a single trip. Therefore, both the PA and ultrasound signals are completely separated in the time domain and therefore can be received without any mixing.

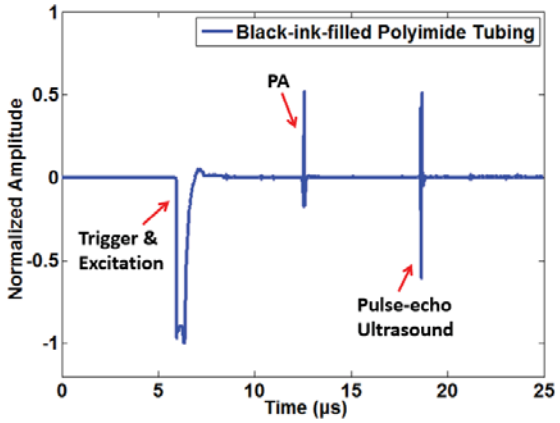

Figure 4. Representative waveform of the received PA and pulse-echo ultrasound signals from a black-ink-filled polyimide tubing in water.

A twisted metal wire with black plastic coating (total diameter $\phi \cong 0.5$ mm) was used as the imaging target, which was immersed in water and embedded inside chicken breast tissue, respectively (Fig. 5). The depth of the wire ranged from 1 to 3 mm. A total area of 8 × 8 mm^2 (marked by the white dashed square in Fig. 5) was scanned with a step size of 100 μm along the two orthogonal directions, and one scan took around 0.5 hr. At each location, the data acquisition was repeated 40 times and the acquired PA & ultrasound signals were averaged to improve the signal-to-noise ratio (SNR) or contrast-to-noise ratio (CNR). To improve the depth of view and reduce the imaging time, the PA and ultrasound data were acquired at five different depths (1.0, 1.5, 2.0, 2.5, and 3.0 mm), which covered the total depth range of the black wire within about 2.5 hrs.

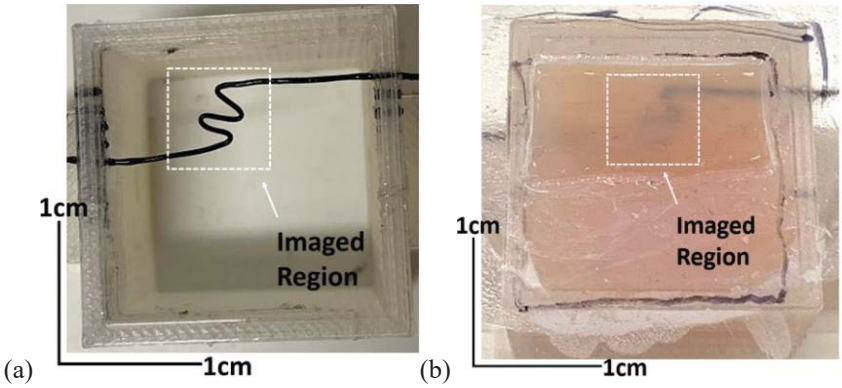

Figure 5. Photos of the black wire (top view) in (a) water, and (b) chicken breast tissue with the depth of 1 ~ 3 mm. The imaged regions are marked by the white dashed squares.

Fig. 6 shows the reconstructed 3D PA and ultrasound images of the black wire in water, which were merged from the data in focal zone at each scanning depth. The normalized signal amplitude of each pixel is indicated by the color bar. The contrast-to-noise ratio (CNR) of the PA and ultrasound images at the different scanning depth is around 36 dB and 30 dB, respectively. The two CNRs remain almost constant, which is due to the weak optical & acoustic absorption and scattering of the water at a depth of a few mm. The slight variation of the CNR is mainly caused by the different tilting angles of the black wire section in the focal zone.

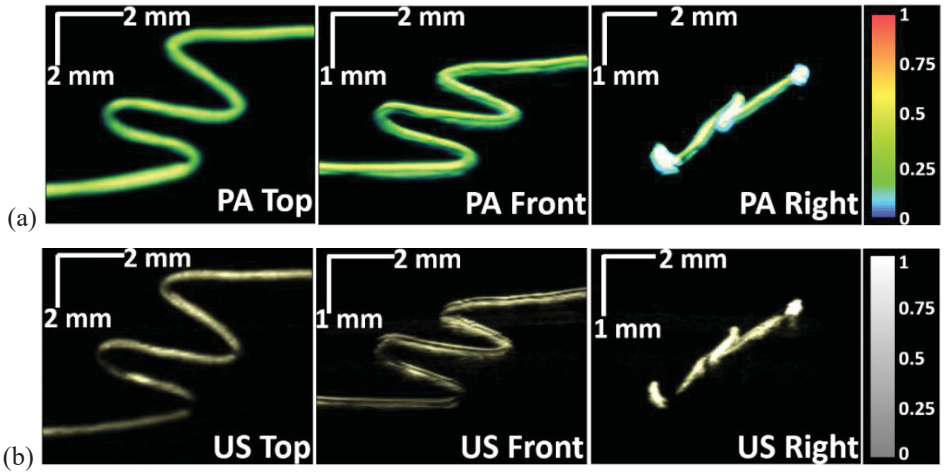

Figure 6. The reconstructed 3D (a) PA and (b) pulse-echo ultrasound images of the black wire in water from three different views. The scale bar represents the normalized signal amplitude. US: ultrasound.

Fig. 7 shows the reconstructed 3D PA and ultrasound images of the black wire in chicken breast tissue. As shown in the PA images (Fig. 7 (a)), the strength of the PA signals gradually drops at larger penetration depths due to the increased optical absorption and more importantly, the optical scattering in chicken breast tissue. The PA contrast-to-noise ratio (CNR) decreases from 33.4 dB (when the top part is in focus) to 25.3 dB (when the bottom part is in focus). Nevertheless, the target at each scanning depth is resolved clearly, and the whole wire across the imaging depth could still be easily differentiated. In contrast, as shown in the ultrasound images, CNR remains around 20 dB at different imaging depths (Fig. 7 (b)), which is lower than that in water. This can be explained by the low acoustic scattering but strong attenuation in the chicken breast tissue.

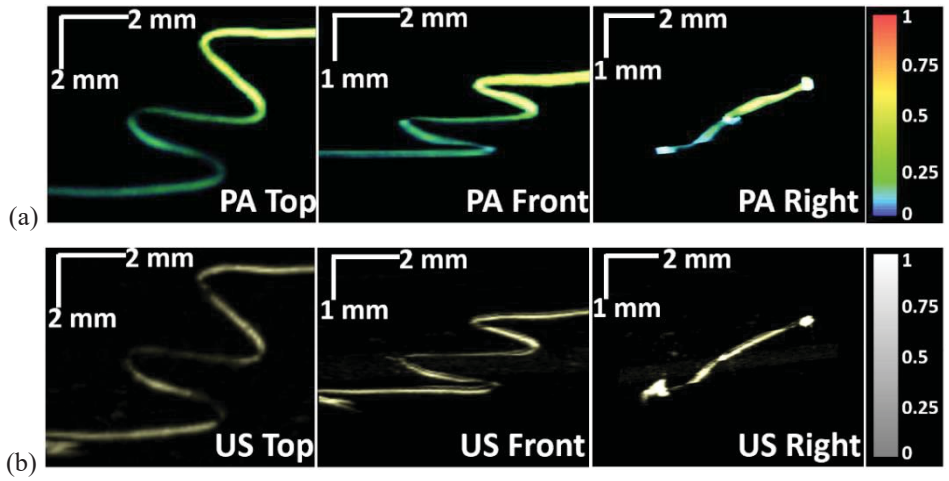

Figure 7. The reconstructed 3D (a) PA and (b) pulse-echo ultrasound images of the black wire in chicken breast tissue from three different views. A tiny air bubble appeared near the lower end of the wire in the ultrasound images, which is invisible in the PA images. The scale bar represents the normalized signal amplitude. US: ultrasound.

For *in-vivo* imaging, a 4-mm-length cross section (B-scan) of a mouse tail (Fig. 8 (a)) was imaged. The lab animal protocol for this work was approved by the University Laboratory Animal Care Committee of Texas A&M University. The tail hair was gently removed before the imaging. Sixteen scans with a lateral step size of 40 μm were repeated at the same cross section with 0.3-mm difference in depth, and the B-scan PA & ultrasound images were reconstructed by merging the data from the focal zone at each different depth (Fig. 8 (b). The PA image (in red, with CNR ~ 28.9 dB) clearly shows the top skin & muscle as well as the dorsal & lateral veins of the mouse tail, while the skin surface pattern and inner structures of the mouse tail are revealed in the ultrasound image (in light blue, with CNR ~ 26.8 dB).

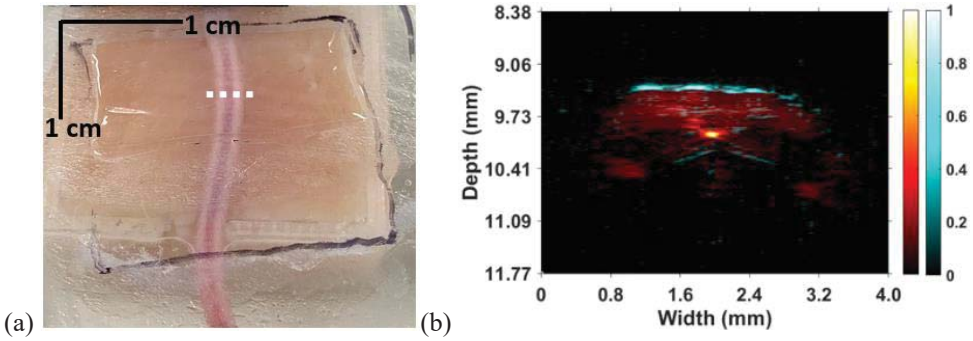

Figure 8. (a) The photo of the imaged mouse tail, where the imaged cross section is marked by the white dashed line. (b) The combined B-scan PA (in red) and pulse-echo ultrasound (in light blue) images of the mouse tail.

5. SUMMARY AND CONCLUSION

In summary, a dual-modal PAM and UM based on an optically-transparent focused PVDF transducer has been demonstrated. With a high NA, a wide acoustic bandwidth, and good optical transparency, the transducer can provide a small acoustic focal spot without light blockage, thereby enabling a simple PAM and UM setup with good acoustic resolution and sensitivity. Such capabilities can be useful for the development of compact PAM and UM systems for handheld, wearable, and even endoscopic imaging applications.

ACKNOWLEDGMENTS

This work is supported in part by awards (NRI-1925037 and CBET-2036134) from the National Science Foundation to JZ. Any opinions, findings, conclusions, or recommendations presented are those of the authors and do not necessarily reflect the views of the National Science Foundation. The authors are grateful to the staff at the Comparative Medicine Program (CMP) at Texas A&M University for assistance in animal handling.

REFERENCES

[1] Wang, L. V., [Photoacoustic imaging and spectroscopy], CRC press (2017).

[2] Wang, L. V. and Yao, J., "A practical guide to photoacoustic tomography in the life sciences," Nature methods 13(8), 627 (2016).

[3] Maslov, K., Stoica, G. and Wang, L. V., "In vivo dark-field reflection-mode photoacoustic microscopy," Optics letters, 30(6), 625-627 (2005).

[4] Wang, L., Maslov, K. I., Xing, W., Garcia-Uribe, A. and Wang, L. V., "Video-rate functional photoacoustic microscopy at depths," Journal of biomedical optics, 17(10), 106007 (2012).

[5] Jeon, S., Kim, J. and Kim, C., "In vivo switchable optical-and acoustic-resolution photoacoustic microscopy," In Photons Plus Ultrasound: Imaging and Sensing 2016, 9708. International Society for Optics and Photonics, 970845 (2016).

[6] Li, L., Yeh, C., Hu, S., Wang, L., Soetikno, B.T., Chen, R., Zhou, Q., Shung, K.K., Maslov, K.I. and Wang, L.V., "Fully motorized optical-resolution photoacoustic microscopy," Optics letters, 39(7), 2117-2120 (2014).

[7] Chen, R., He, Y., Shi, J., Yung, C., Hwang, J., Wang, L. V. and Zhou, Q., "Transparent High-Frequency Ultrasonic Transducer for Photoacoustic Microscopy Application," IEEE transactions on ultrasonics, ferroelectrics, and frequency control, 67(9), 1848-1853 (2020).

[8] Ilkhechi, A. K., Ceroici, C., Dew, E. and Zemp, R., "Transparent capacitive micromachined ultrasound transducer linear arrays for combined realtime optical and ultrasonic imaging," Optics Letters, 46(7), 1542-1545 (2021).

[9] Ilkhechi, A. K., Ceroici, C., Li, Z. and Zemp, R., "Transparent capacitive micromachined ultrasonic transducer (CMUT) arrays for real-time photoacoustic applications," Optics express, 28(9), 13750-13760 (2020).

[10] Park, S., Kang, S. and Chang, J. H., "Optically transparent focused transducers for combined photoacoustic and ultrasound microscopy," Journal of Medical and Biological Engineering, 40, 707-718 (2020).

[11] Park, J., Park, B., Kim, T. Y., Jung, S., Choi, W. J., Ahn, J., Yoon, D.H., Kim, J., Jeon, S., Lee, D., Yong, U., ... and Kim, C., "Quadruple ultrasound, photoacoustic, optical coherence, and fluorescence fusion imaging with a transparent ultrasound transducer," Proceedings of the National Academy of Sciences, 118(11) (2021).

[12] Fang, C., Hu, H. and Zou, J., "A Focused Optically Transparent PVDF Transducer for Photoacoustic Microscopy," IEEE Sensors Journal, 20(5), 2313-2319 (2019).

[13] Fang, C. and Zou, J., "Acoustic-resolution photoacoustic microscopy based on an optically transparent focused transducer with a high numerical aperture, " Optics letters, 46(13), 3280-3283 (2021).

[14] Olympus, “Ultrasonic Transducers Technical Notes,” http://ru.twn-technology.com/Download/Olympus/Olympus%20transducers%20EN.pdf (2011).